Magnetic edge states in graphene in nonuniform magnetic fields

Sunghun Park and H.-S. Sim
Department of Physics, Korea Advanced Institute of Science and Technology, Daejeon 305-701, Korea
(Received 15 November 2007; published 28 February 2008)

We theoretically study the electronic properties of a graphene sheet on the xy plane in a spatially nonuniform magnetic field, $B=B_0\hat{z}$ in one domain and $B=B_1\hat{z}$ in the other domain, in the quantum Hall regime, and in the low-energy limit. We find that the magnetic edge states of the Dirac fermions, formed along the boundary between the two domains, have features strongly dependent on whether B_0 is parallel or antiparallel to B_1. In the parallel case, when the Zeeman spin splitting can be ignored, the magnetic edge states originating from the $n=0$ Landau levels of the two domains have dispersionless energy levels contrary to those from the $n\neq 0$ levels. Here, n is the graphene Landau-level index. They become dispersive as the Zeeman splitting becomes finite or as an electrostatic step potential is additionally applied. In the antiparallel case, the $n=0$ magnetic edge states split into electronlike and holelike current-carrying states. The energy gap between the electronlike and holelike states can be created by the Zeeman splitting or by the step potential. These features are attributed to the fact that the pseudospin of the magnetic edge states couples to the direction of the magnetic field. We propose an Aharonov–Bohm interferometry setup in a graphene ribbon for an experimental study of the magnetic edge states.

DOI: 10.1103/PhysRevB.77.075433 PACS number(s): 81.05.Uw, 73.21.−b, 72.15.Gd, 73.63.−b

I. INTRODUCTION

Graphene, a two-dimensional (2D) honeycomb lattice of carbons, has attracted much attention because of its unusual electronic properties. In the low-energy regime, electrons near the two inequivalent valleys, K and K', of its electronic structure can be described by massless Dirac fermions[1,2] and they exhibit half-integer quantum Hall effects,[3,4] in contrast to the quantum Hall effect of the conventional 2D electrons formed in semiconductor heterostructures.[5] The long phase coherence length and mean free path, of micrometer order, measured[6,7] in high-quality graphenes indicate potential applications of a graphene ribbon to coherent nanodevices.

On the other hand, the electron properties of the conventional 2D systems have been investigated in the presence of spatially nonuniform magnetic fields. The nonuniform fields can cause the formation of charateristic current-carrying edge states[8,9] along the region of field gradient, which correspond to the semi $\vec{\nabla}B\times\vec{B}$ drift motion. These states have been referred[10] to as *magnetic edge states* in analogy to the edge states,[11] corresponding to the $\vec{E}\times\vec{B}$ drift along sample boundaries. Their features have been studied experimentally.[12] The nonuniform fields can form various magnetic structures such as magnetic steps,[13–15] magnetic quantum dots,[10,16,17] magnetic rings,[18] magnetic superlattices,[19–21] etc., and play the role of characteristic barriers and resonators for electron transport,[22,23] the properties of which are very different from those formed by an electrostatic gate potential.

A graphene sheet may provide a good experimental system for studying the effects of the nonuniform magnetic fields as a nonuniform-field configuration can be effectively generated by applying a uniform field to a curved sheet.[24] In addition, the Dirac fermions in graphene can have interesting properties under nonuniform fields,[25] which may be different from those of the magnetic edge states in the conventional 2D systems, since the Dirac fermions have electronlike, zero-mode, and holelike Landau levels, as well as the pseudospins representing the two sublattice sites of the honeycomb lattice. Therefore, it may be valuable to study the electron properties of graphene in a nonuniform magnetic field, which is the aim of the present work.

In this theoretical work, we study the electronic structures of a graphene sheet (on the xy plane) in a spatially nonuniform magnetic field of step shape, $\vec{B}=B_0\hat{z}$ for $x<0$ and $\vec{B}=B_1\hat{z}$ for $x>0$, in the integer quantum Hall regime, based on a noninteracting-electron approach. By solving the Dirac equation, we first investigate the low-energy properties of the magnetic edge states formed along the boundary ($x=0$) between the two domains with different fields B_0 and B_1 when the Zeeman effect is negligible. They are found to strongly depend on whether B_0 is parallel or antiparallel to B_1. In the palallel case of $\gamma\equiv B_1/B_0>0$, the magnetic edge states originating from the $n=0$ Landau levels of the two domains are dispersionless contrary to those from the $n\neq 0$ levels, where n is the Landau-level index. In the antiparallel case of $\gamma<0$, the $n=0$ magnetic edge states split into electronlike and holelike levels near the boundary. These features, which are absent in the magnetic edge states of the conventional 2D electrons, are attributed to the fact that the pseudospin of the magnetic edge states couples to the direction of the magnetic field. On the other hand, the features of the $n\neq 0$ magnetic edge states are similar to those of the conventional cases.

We further study the magnetic edge states in the presence of an additional electrostatic step potential, $V(x)=V_0$ for $x<0$ and $V(x)=V_1$ for $x>0$. For $\gamma>0$, the $n=0$ magnetic edge states become dispersive, while for $\gamma<0$ an energy gap becomes created around the bipolar region in the spectrum of the magnetic edge states. Similar features can be found when the Zeeman spin splitting is finite, because in the nonuniform field of step shape, the Zeeman effect behaves as the step potential.

Finally, we suggest an interferometry setup formed in a graphene ribbon for experimental study. In this setup, the

magnetic edge states can provide partial paths of a full Aharonov–Bohm interference loop, therefore the properties of the magnetic edge states such as the gap of their energy spectra can be investigated. We numerically calculate the transmission probability through the setup by using the tight-binding method and the Green function technique.[30–32] The results are consistent with the features of the magnetic edge states obtained by solving the Dirac equation. We also derive the transmission probability, based on the scattering matrix formalism, and use it to analyze the numerical results.

This paper is organized as follows. The magnetic edge states are studied without and with the electrostatic step potential in Secs. II and III, respectively. The Zeeman spin splitting is considered in Sec. IV, and the graphene interferometry is suggested and investigated in Sec. V. In Sec. VI, this work is summarized. Throughout this work, we ignore the intervalley mixing due to the nonuniform field, the validity of which is discussed in Appendix A. In Appendix B, we derive the transmission probability, which may be applicable to other graphene interferometry setups with a slight modification.

II. MAGNETIC EDGE STATES

We consider a graphene sheet (on the xy plane) in the nonuniform magnetic field of the step configuration,

$$\vec{B}(x) = \begin{cases} B_0\hat{z}, & x<0 \\ B_1\hat{z}, & x>0, \end{cases} \tag{1}$$

in the integer quantum Hall regime. Without loss of generality, B_0 is chosen to be positive and $\gamma \equiv B_1/B_0$ is either positive or negative. This configuration may be realized with field gradient dB/dx less than 10^4 T Å^{-1} and with not-too-strong field strengths B_0 and $|B_1|$ (less than, e.g., 100 T). In this case, the mixing between the K and K' valleys due to the nonuniform field can be ignored (see Appendix A), and the electrons in each valley can be described separately by the Dirac equation,

$$[v\vec{\sigma}_J \cdot \vec{\Pi} + V(x)]\Psi_J = E\Psi_J, \tag{2}$$

in the low-energy approximation. Here, $J \in \{K, K'\}$ is the valley index, $v = \sqrt{3}at/2\hbar \sim 10^6$ m s^{-1}, a is the lattice constant of graphene, t is the hopping energy between two nearest-neighbor sites, $\vec{\sigma}_K = (\sigma_x, \sigma_y)$ and $\vec{\sigma}_{K'} = (-\sigma_x, \sigma_y)$ are constructed by the Pauli matrices, $\vec{\Pi} \equiv \vec{p} + e\vec{A}$, $\vec{p}$ is the momentum measured relative to the valley center (K or K' point), $\vec{A}$ is the vector potential, and $e(>0)$ is the electron charge. The electrostatic potential $V(x)$ applied to the sheet must be a smoothly varying function of x. The detailed form of $V(x)$ will be specified in Sec. III. The components of the pseudospinor Ψ_J represent the wave functions of the two sublattice sites (denoted by A and B hereafter) of a unit cell of graphene. The Dirac equations for the K and K' valleys are connected to each other by a unitary transformation $U = \sigma_y$. This feature suggests that the two equations have the same energy levels and that their wave functions have the relation, $\Psi_{K'} = U\Psi_K$. Therefore, it is enough to solve the Dirac eqaution for the K valley only.

Before studying the nonuniform-field cases, we briefly discuss the case of a uniform magnetic field with strength B. In this case, the Landau levels are found[3] to be

$$E_n = \mathrm{Sgn}(n) v\sqrt{2|n|\hbar eB}, \tag{3}$$

where $n = 0, \pm 1, \pm 2, \ldots$, is the Landau-level index. The levels with $n>0$ are often referred to as electronlike, while those with $n<0$ as holelike. In fact, one can obtain the Landau levels from the square of the Dirac Hamiltonian,

$$E_n^2 = 2\hbar e v^2 B(m + 1/2 \pm 1/2) \tag{4}$$

for the K valley, with $|n| = m + 1/2 \pm 1/2$ and $m = 0, 1, 2, \ldots$. For a later discussion, it is worthwhile to analyze E_n^2. The harmonic term with $B(m+1/2)$ is nothing but the Landau level of the conventional 2D electrons, while the next term $\pm B/2$ can be interpreted as the effective-Zeeman effect of the pseudospin; $B/2$ for pseudo-spin-up and $-B/2$ for pseudo-spin-down. Each Landau level with $n \neq 0$ is composed of the pseudo-spin-up (with $m = |n| - 1$) and pseudo-spin-down (with $m = |n|$) states, while the $n=0$ level comes only from the pseudo-spin-down (up) states with $m=0$ in the K (K') valley. The $n=0$ level is independent of B as the harmonic and effective-Zeeman terms exactly cancel each other.

Turning back to the nonuniform field in Eq. (1), we consider the case without electrostatic potential, $V(x)=0$, in this section. We choose the vector potential as $\vec{A}(x) = B_0 x\hat{y}$ for $x<0$ and $\vec{A}(x) = B_1 x\hat{y}$ for $x>0$. This choice of $\vec{A}$ is useful, as the solution of Eq. (2) for the K valley can be written as $\Psi_K^\dagger(x) = e^{-iky}\Phi^\dagger(x) = e^{-iky}(\phi_A^*(x), \phi_B^*(x))$, where ϕ_j is the wave function of the sublattice site $j \in \{A, B\}$ and $\hbar k$ is the eigenvalue of p_y. Hereafter, we will measure energy and length in units of E_1 ($\equiv \sqrt{2\hbar v^2 eB_0}$) and l_B ($\equiv \sqrt{\hbar/eB_0}$), where l_B and E_1 are the magnetic length and the energy gap between the $n=0$ and $n=1$ Landau levels, respectively, of the bulk region with B_0. In these units, the Landau levels are equal to $\sqrt{n}$ at $x \ll -1$, while they are equal to $\mathrm{Sgn}(n)\sqrt{|\gamma| n}$ at $x \gg 1/\sqrt{|\gamma|}$. Then the equation for $\phi_{j=A,B}$ is found to be

$$-\frac{d^2\phi_{j,k}(x)}{dx^2} + 2[V_{\mathrm{eff}}^j(x,k) - E_{n,k}^2]\phi_{j,k}(x) = 0. \tag{5}$$

The effective potential[10] V_{eff}^j is harmonic,

$$V_{\mathrm{eff}}^j(x,k) = \begin{cases} \frac{1}{2}(x+k)^2 + s_j\frac{1}{2}, & x<0 \\ \frac{1}{2}(\gamma x + k)^2 + s_j\frac{\gamma}{2}, & x>0, \end{cases} \tag{6}$$

where $s_{j=A} = 1$ and $s_{j=B} = -1$. Equation (5) has the form of the usual Schrödinger equation with potential V_{eff}^j and eigenvalue $E_{n,k}^2$. Therefore, V_{eff}^j is useful for understanding $\phi_{j,k}(x)$ and $E_{n,k}$. The form of V_{eff}^j in Eq. (6) shows that the pseudospin (s_j) couples to the *direction* (γ) of the magnetic field.

The solution $\phi_{j,k}^<$ of Eq. (5) for $x<0$ can be expressed in terms of the parabolic cylinder functions[26] $D_\nu(z)$ as

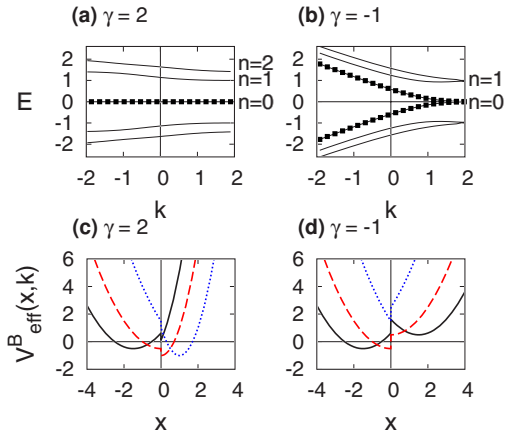

FIG. 1. (Color online) Upper panels: Energy spectra $E_{n,k}$ for (a) $\gamma=2$ and (b) $\gamma=-1$. The energy levels of the $n=0$ magnetic edge states are highlighted by the filled squares. For $\gamma>0$, the $n=0$ levels are dispersionless, while they split into electronlike and holelike levels for $\gamma<0$. Lower panels: Effective potential $V_{\text{eff}}^{j=B}(x,k)$ in Eq. (6) for (c) $\gamma=2$ and (d) $\gamma=-1$. Different values of $k=1.5$ (solid line), 0 (dashed), and -2 (dotted) are chosen. Energy and length are measured in units of E_1 $(\equiv\sqrt{2\hbar v^2 eB_0})$ and l_B $(\equiv\sqrt{\hbar/eB_0})$, respectively.

$$\begin{pmatrix}\phi^{<}_{A,k}\\ \phi^{<}_{B,k}\end{pmatrix}\propto\begin{pmatrix}iED_{E^2-1}[-\sqrt{2}(x+k)]\\ D_{E^2}[-\sqrt{2}(x+k)]\end{pmatrix}. \tag{7}$$

On the other hand, for $x>0$, the solution $\phi^{>}_{j,k}$ is found to be dependent on the sign of γ, i.e., on whether B_1 is either parallel or antiparallel to B_0. For $\gamma>0$,

$$\begin{pmatrix}\phi^{>}_{A,k}\\ \phi^{>}_{B,k}\end{pmatrix}\propto\begin{pmatrix}-i\dfrac{E}{\sqrt{\gamma}}D_{(E^2/\gamma)-1}\left[\sqrt{2\gamma}\left(x+\dfrac{k}{\gamma}\right)\right]\\ D_{E^2/\gamma}\left[\sqrt{2\gamma}\left(x+\dfrac{k}{\gamma}\right)\right]\end{pmatrix}, \tag{8}$$

and for $\gamma<0$,

$$\begin{pmatrix}\phi^{>}_{A,k}\\ \phi^{>}_{B,k}\end{pmatrix}\propto\begin{pmatrix}D_{E^2/|\gamma|}\left[\sqrt{2|\gamma|}\left(x+\dfrac{k}{\gamma}\right)\right]\\ -i\dfrac{E}{\sqrt{|\gamma|}}D_{(E^2/|\gamma|)-1}\left[\sqrt{2|\gamma|}\left(x+\dfrac{k}{\gamma}\right)\right]\end{pmatrix}. \tag{9}$$

The energy eigenvalue $E_{n,k}$ can be obtained under the boundary condition of the continuity of the wave functions in Eqs. (7)–(9) at $x=0$. $E_{n,k}$ is drawn in Fig. 1 for the two cases of $\gamma=2$ and $\gamma=-1$. These two specific cases of γ are enough to understand the characteristics of the magnetic edge states.

The energy levels strongly depend on whether B_1 is parallel or antiparallel to B_0. In the parallel case of $\gamma>0$, for each n the energy levels gradually change from $\text{Sgn}(n)\sqrt{|n|}$ to $\text{Sgn}(n)\sqrt{\gamma|n|}$ as k decreases from positive to negative values [see the $\gamma=2$ case in Fig. 1(a)]. This feature can be understood from the effective potential [see Eq. (6) and Fig. 1(c)]. As k increases from negative to positive values, the bottom of $V_{\text{eff}}^{j}(x)$ moves from the region with B_1 to that with B_0, passing the boundary $x=0$ around $k=0$. Therefore, for $k\ll 0$, the eigenstates have the Landau levels $\text{Sgn}(n)\sqrt{\gamma|n|}$ and localize around $x=-k/\gamma$ (in the unit of l_B), while for $k\gg 0$, they have $\text{Sgn}(n)\sqrt{|n|}$ and localize around $x=-k$. Around $k=0$, the two levels of $\text{Sgn}(n)\sqrt{\gamma|n|}$ and $\text{Sgn}(n)\sqrt{|n|}$ connect smoothly and the corresponding states are localized around $x=0$. These states have been called[10] magnetic edge states and they can carry current along the boundary $x=0$.

Contrary to the corresponding states in the conventional 2D systems, the magnetic edge states in graphene have the following different features for $\gamma>1$. First, the edge states with $n>0$ behave as electrons, with dispersion $dE_n/dk<0$, while those with $n<0$ behave as holes, with $dE_n/dk>0$. Second, the edge states with $n=0$ are dispersionless and carry no current *regardless* of $\gamma(>0)$. These features come from the nature of the Dirac fermions. Especially, the second one can be understood from the fact that for $\gamma>0$, the effective-Zeeman and harmonic contributions to $E^2_{n=0}$ cancel each other on both sides of $x=0$, as discussed in Eq. (4) and as shown in the term of V^j_{eff} representing the coupling of pseudospin to field direction [see Eq. (6)]. The case of $0<\gamma<1$ can be understood in a similar way.

Next, we discuss the case of $\gamma<0$, which is very different from the $\gamma>0$ case [see Fig. 1(b)]. For large positive k, the eigenstates have the Landau levels of $\text{Sgn}(n)\sqrt{|n|}$ or $\text{Sgn}(n)\sqrt{|\gamma n|}$, while for large negative $k(\ll 0)$, their energy either increases (shows electronlike behavior) or decreases (holelike). This feature can be understood from $V^j_{\text{eff}}(x,k)$. As shown in Fig. 1(d), for large positive k, the two local harmonic wells of $V^j_{\text{eff}}(x,k)$ occur far from the boundary of $x=0$, resulting in the Landau levels that are localized in each well. As k decreases to negative values, the two local wells move toward $x=0$ and merge into a single well (not harmonic anymore) at $x=0$, and then the bottom of the merged well increases. Therefore, the eigenstates with $k\lesssim 0$ are magnetic edge states localized at $x=0$ and they can carry current along $x=0$. They are either electronlike $(dE_{n\geqslant 0}/dk<0)$ or holelike $(dE_{n\leqslant 0}/dk>0)$. One can estimate their group velocity for $k\ll 0$ as $(1/\hbar)dE_n/dk\sim\pm v$ from the minimum value of the merged well of V^j_{eff}, where $+$ $(-)$ stands for the hole (electron)-like states. In the case of $\gamma<0$, where the magnetic fields B_0 and B_1 are antiparallel, the eigenstates in $n\neq 0$ Landau levels correspond to classical motions, so-called snake orbits,[8–10,14] while those in the $n=0$ level have no clear correspondence to classical motions as they have both electron and hole characters.

For $\gamma<0$, the effective-Zeeman contribution to E^2_n has the opposite sign between the domains of $x>0$ and $x<0$, as shown in Eq. (6). This coupling of pseudospin to field direction causes an energy barrier at $x=0$. For example, a pseudospin-down state has larger effective-Zeeman contribution at $x>0$ than at $x<0$. As a result, as k decreases, the magnetic edge state becomes more confined around $x=0$ due to the effective-Zeeman barrier. This pseudospin feature, which enhances the splitting into electronlike and holelike states, is absent in the magnetic edge states of the conventional 2D electrons.

III. MAGNETIC EDGE STATES IN AN ELECTROSTATIC STEP POTENTIAL

In this section, we consider an additional electrostatic potential $V(x)$ of step shape,

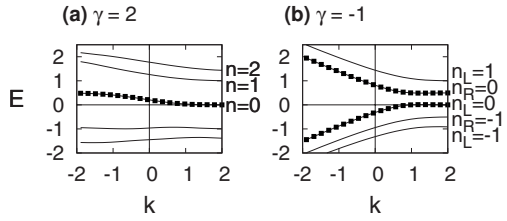

FIG. 2. The same as in Fig. 1 but in the presence of the step potential $V(x)$ with $V_0=0$ and $V_1=0.5$. For $\gamma=-1$, the energy levels are labeled by n_L and n_R, which are the indices of the Landau levels localized at $x\ll -1$ and at $x\gg 1/\sqrt{|\gamma|}$, respectively (see text). The $n=0$ levels become dispersive for $\gamma>0$, while the energy gap opens between electronlike ($n_R=0$) and holelike levels ($n_L=0$) for $\gamma<0$.

$$V(x)=\begin{cases} V_0, & x<0 \\ V_1, & x>0, \end{cases} \tag{10}$$

to the nonuniform magnetic field in Eq. (1). Here, V_0 and V_1 are constants. This potential gives rise to a characteristic modification of the $n=0$ magnetic edge states, such as the creation of an energy gap for $\gamma<0$, as will be seen below. Moreover, the modification is directly applicable to the case where the Zeeman spin splitting is finite, as will be studied in Sec. IV.

The step potential $V(x)$ is assumed to be smoothly varying in the length scale of the lattice constant a. Then, we can still ignore the intervalley mixing and solve the Dirac equation in Eq. (2) in the same way as above. In Fig. 2, choosing $V_0=0$ and $V_1=0.5$ (in the units of E_1 and l_B), we draw the energy spectra of the magnetic edge states for $\gamma=2$ and $\gamma=-1$.

The features of the energy spectra are discussed below. For $\gamma>0$, the eigenstates with large positive (negative) k have the Landau levels shifted by V_0 (V_1) and do not carry current, while the magnetic states around $k=0$ have the energy smoothly connecting the Landau levels of the large positive and negative k's. We point out that the $n=0$ magnetic edge states carry current due to the potential step $V(x)$. On the other hand, for $\gamma<0$, the eigenstates with large positive k have the Landau levels shifted by V_0 or V_1, depending on whether they are localized in the bulk region of $x<0$ or $x>0$. For convenience, we introduce the Landau-level indices n_L and n_R for those localized in $x<0$ and in $x>0$, respectively. In this case, the energy levels with $n=0$ split, opening the *energy gap* between the electronlike and holelike magnetic edge states contrary to the case without the step potential. For $\gamma=-1$ and $V_1-V_0=0.5$, the gap size is the same as the step height V_1-V_0.

We further study the energy gap with varying height V_1-V_0 for $\gamma=-1$. In Fig. 3, we choose $V_1-V_0=1.5$, which is larger than the energy spacing between the $n=0$ and $n=1$ Landau levels, contrary to the case of Fig. 2(b) where the height (=0.5) is smaller. In this case, the energy gap of the magnetic edge states occurs between the $n_L=1$ and $n_R=-1$ Landau levels. Moreover, the gap size is no longer the same as the step height, but corresponds to the energy difference (=0.5) between the $n_L=1$ and $n_R=-1$ levels.

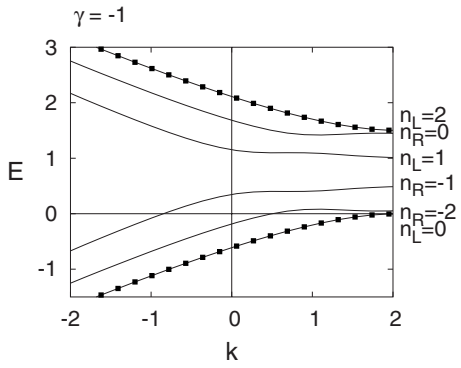

FIG. 3. The same as in Fig. 2(b) but with $(V_0,V_1)=(0,1.5)$.

The above feature can be understood as follows. For $\gamma=-1$, the effective Hamiltonian in Eq. (2) is odd under the inversion operator $\mathcal{R}_{\rm inv}$, $\mathcal{R}_{\rm inv}\vec{x}=-\vec{x}$,

$$\begin{aligned}\mathcal{R}_{\rm inv}\left[v\vec{\sigma}_J\cdot\vec{\Pi}+V(x)-\frac{V_0+V_1}{2}\right]\mathcal{R}_{\rm inv}\mathcal{R}_{\rm inv}\Psi_J \\ =-\left[v\vec{\sigma}_J\cdot\vec{\Pi}+V(x)-\frac{V_0+V_1}{2}\right]\mathcal{R}_{\rm inv}\Psi_J \\ =\left(E-\frac{V_0+V_1}{2}\right)\mathcal{R}_{\rm inv}\Psi_J.\end{aligned} \tag{11}$$

This property is consistent with the facts that the gap center is located at $E_c\equiv(V_0+V_1)/2$ and that the gap size is determined by the energy difference between the Landau levels just below and above E_c. Similar to the case in Fig. 1, it can also be understood[27] from $V_{\rm eff}^j$ that the states with $E>E_c$ are electronlike, while those with $E<E_c$ are holelike.

IV. ZEEMAN SPLITTING OF THE MAGNETIC EDGE STATES

So far, we have ignored the spin degree of freedom. Recently, Abanin *et al.* discussed[33] that, in graphene, the Zeeman splitting can be smaller than the Landau energy gap only by the factor of about 10^{-1}, due to the exchange interaction, and that it can play an important role in the edge-channel transport in the quantum Hall regime. In this section, we discuss the effect of the Zeeman splitting on the magnetic edge states.

In the nonuniform field $B(x)$ in Eq. (1), the Zeeman splitting behaves as a spin-dependent step potential,

$$V_s^Z(x)=s\Delta_Z B(x), \tag{12}$$

where $\Delta_Z=g^*\mu_B/E_1$, $s=1/2$ ($s=-1/2$) for spin-up (down) electrons, and μ_B is the Bohr magneton. The exchange enhancement[33] of the g factor can be taken into account in g^*. We assume that $V_s^Z\ll 1$ for convenience.

The Zeeman splitting can be considered as the spin-dependent shift of the step potential, $V(x)\to V(x)+V_s^Z(x)$. The resulting magnetic edge states can easily be understood from the features discussed in Sec. III. In Fig. 4, we draw schematic energy dispersions of the $n=0$ magnetic edge

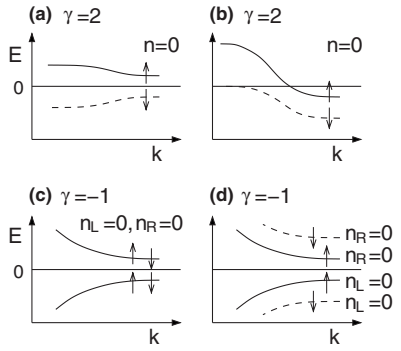

FIG. 4. Schematic spin-dependent energy dispersion of the $n=0$ magnetic edge states in the presence of the Zeeman splitting, $2|V_s^Z|=0.2$. We choose the parameters (γ, V_0, V_1) as (a) (2,0,0), (b) (2,−0.2,0.2), (c) (−1,0,0), (d) (−1,−0.2,0.2).

states; the extension to $n\neq 0$ states is trivial. For $\gamma>0$, the $n=0$ states are dispersive near $x=0$, as shown in Figs. 4(a) and 4(b). The energy difference between the spin-up and -down states varies from $\gamma\Delta_Z$ to Δ_Z as k increases. The average value of the spin-up and -down energy levels is shifted by V_0 (V_1) at large positive (negative) k. On the other hand, for $\gamma<0$, the energy gap of the $n=0$ magnetic edge states exists even without the electrostatic step potential [see Fig. 4(c)]. For both the cases of $\gamma>0$ and $\gamma<0$, the sign of the drift velocity $(\sim dE/dk)$ is either positive or negative, depending on Δ_Z, V_0, and V_1. These spin-split dispersions show that spin-polarized current can emerge between two magnetic domains.

V. GRAPHENE INTERFEROMETRY

In this section, we propose an interferometry setup for studying magnetic edge states in a graphene ribbon. We focus on the case of $\gamma=-1$ in Fig. 2(b) and demonstrate that the energy gap of the magnetic edge states can be directly studied by observing the Aharonov–Bohm interference of the setup. The interferometry setup is useful as well for the other cases of γ.

We consider a ribbon with armchair edge; a setup with zigzag edge will show a similar result. The ribbon consists of three parts; the current source in the left, the middle scattering region, and the drain in the right. A nonuniform magnetic field is applied such that $B=B_0\hat{z}$ in the source and drain, while $B=\tilde{B}_0\hat{z}\simeq -B_0\hat{z}$ in the middle region (see Fig. 5). At the same time, a constant electrostatic potential $V_0=0$ is applied to the source and drain, while $V_1=0.5$ in the middle region. Then, the magnetic edge states form along the left and right boundaries $\overline{ab}$ and $\overline{cd}$ of the middle region, while along each boundary of the ribbon, there is one edge channel, which is formed as a mixture of the contribution of the K and K' valleys.[28] The magnetic edge states are the same as those studied in Fig. 2(b), when their position separates from the ribbon edge by more than the scale of magnetic length, $l_B\equiv\sqrt{\hbar/eB_0}$, so that the overlap between the magnetic edge states and the ribbon-edge channels is negligible. Note that at each of the scattering points $a-d$ in Fig. 5(a), the number of

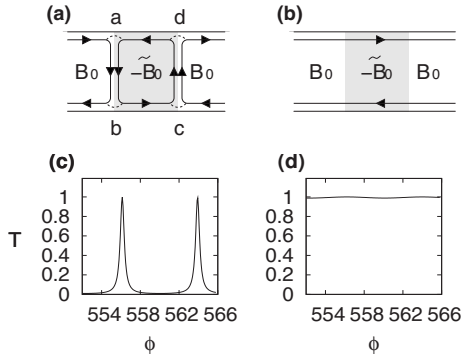

FIG. 5. Upper panel: Schematic diagram of a graphene-ribbon interferometry, which consists of the left (with magnetic field B_0), middle (with $-\tilde{B}_0$), and right (with B_0) regions. There is one edge channel along the ribbon edges, while there can be magnetic edge states along the left and right boundaries, $\overline{ab}$ and $\overline{cd}$, of the middle region, depending on the energy of the states and the field configuration of $(B_0,-\tilde{B}_0)$. In (a), there appear two magnetic edge states along each boundary, and thus the Aharonov–Bohm interference, while no state and no interference exists in (b). Lower panel: Aharonov–Bohm effect in the transmission T through the interferometry as a function of the Aharonov–Bohm flux ϕ. The case of (a) is plotted in (c), while that of (b) in (d).

the incoming channels is the same as that of the outgoing channels, so that the current is conserved.

The formation of the magnetic edge states depends on energy. In the energy range $\in[0.5,1]$ of Fig. 2(b), where each valley supports only one magnetic edge channel, one has the edge-channel transport shown in Fig. 5(a). In this case, there appears an Aharonov–Bohm loop around the middle region, which is supported by the two counterpropagating edge channels along the upper and lower ribbon edges and by the magnetic edge states along the boundaries $\overline{ab}$ and $\overline{cd}$. As a function of $\tilde{B}_0$, one can observe the Aharonov–Bohm interference in the transmission through the setup. On the other hand, in the energy range $\in[0,0.5]$, where there is no magnetic edge state along $\overline{ab}$ and $\overline{cd}$ [see Fig. 5(b)], no Aharonov–Bohm interference can be observed. Therefore, the Aharonov–Bohm loop can be formed, depending on whether the magnetic edge channels exist along the boundaries $\overline{ab}$ and $\overline{cd}$. This property allows one to measure the gap of the magnetic edge states by varying the energy of the incoming edge channel and by modulating $\tilde{B}_0$.

We confirm the above proposal numerically by calculating the transmission probability $T(E)$ through the setup, using the tight-binding method[29] and the Green's function approach.[30,31] Here, we skip the details of the method and instead refer Refs. 23 and 32. The effect of the magnetic field is taken into account by the Peierls phase. The strength of B_0 is set to be about 800 T. At the boundaries $\overline{ab}$ and $\overline{cd}$, the magnetic field spatially varies linearly from B_0 to $\tilde{B}_0$ over the length scales of $3l_B$. We choose the ribbon width $|\overline{ab}|$ and the width $|\overline{bc}|$ of the middle region to be about $15l_B$ and $30l_B$, respectively, so that we can ignore the overlap between the edge channels propagating oppositely to each other.

In Fig. 5, we plot $T(E)$ for $E=0.65$ and $E=0.35$ as a function of the Aharonov–Bohm flux $\phi\equiv 2\pi|\tilde{B}_0|S/\phi_0$, where

E is the energy of the incoming states to the setup, S is the area of the middle region, and $\phi_0=h/e$ is the flux quantum. As expected, for $E=0.65$, one has the interference, while none for $E=0.35$. This confirms the proposal discussed above.

Finally, we briefly analyze the numerical result for $E=0.65$ in Fig. 5(a). The period of the Aharonov–Bohm oscillation is found to be $\Delta\phi=7.8=1.24(2\pi)$. The fact that $\Delta\phi/2\pi$ is larger than 1 indicates that the actual Aharonov–Bohm loop has smaller area than S, which is reasonable. The line shape of the interference can be analyzed using the expression of T in Eq. (B7) derived in Appendix B. The line shape is well fitted by Eq. (B7) with parameters of $\alpha=\beta=0.5$ and $t_a=t_b=t_c=t_d=0.23$. From this fitting, one can get the information of the scattering between the edge channels along the ribbon edges and the magnetic edge channels along ab and cd.

VI. SUMMARY

We have studied the magnetic edge states formed along the boundary between the two domains with different magnetic fields B_0 and B_1 in graphene. It turns out that the magnetic edge states have very different features from those of the conventional 2D electrons, since the former have a pseudospin which couples to the direction of the magnetic field. As a result, the $n=0$ magnetic edge states are dispersionless for $\gamma\equiv B_1/B_0>0$, while they split into electronlike and holelike current-carrying states for $\gamma<0$. The Zeeman spin splitting or the additional electrostatic step potential can make the $n=0$ states dispersive for $\gamma>0$ and open an energy gap in the bipolar region for $\gamma<0$. These features show an interesting manifestation of the Dirac fermions in graphene, and the magnetic edge states can play a special role in the transport of the Dirac fermions in a nonuniform magnetic field, such as spin-polarized current along the boundaries of magnetic domains.

Note added. During the preparation of this manuscript, we have been aware of two preprints[34,35] where the energy dispersion and current density of the snake states in a nonuniform magnetic field of waveguide shape are studied. Their results partially overlap with our results for the case of $\gamma<0$ in Sec. II.

ACKNOWLEDGMENT

We are supported by the Korean Research Foundation (Grants Nos. KRF-2005-084-C00007 and KRF-2006-331-C00118).

APPENDIX A: INTERVALLEY SCATTERING IN NONUNIFORM MAGNETIC FIELDS

In this section, based on the tight-binding method, we show that the mixing between the K and K' valleys, due to a spatially nonuniform magnetic field, can be ignored when the field strength and the gradient of the field are much smaller than 10^4 T and 10^4 T A^{-1}, respectively, which is achieved in current experimental studies.

We first discuss the matrix elements of the tight-binding Hamiltonian of graphene in the presence of an external magnetic field. For each sublattice site $j=A,B$, the Bloch wave functions of an electron is written as

$$\Phi_{\vec{k}}^{j}(\vec{r})=\frac{1}{\sqrt{N}}\sum_{\vec{R}_j}\exp\left(i\vec{k}\cdot\vec{R}_j-i\frac{e}{\hbar}\int_{\vec{R}_j}^{\vec{r}}\vec{A}\cdot d\vec{r}_1\right)\phi(\vec{r}-\vec{R}_j), \tag{A1}$$

where the sum runs over the potisions $\vec{R}_j$ of site j, N is the number of unit cells, $\vec{A}(\vec{r}_1)$ is the vector potential, $\vec{k}$ is the momentum of the states, and $\phi(\vec{r})$ is the wave function of electrons participating in the π bonding. The matrix element $\langle\Phi_{\vec{k}'}^{B}|H|\Phi_{\vec{k}}^{A}\rangle$ of the tight-binding Hamiltonian for the nearest-neighbor hopping is found to be

$$\langle\Phi_{\vec{k}'}^{B}|H|\Phi_{\vec{k}}^{A}\rangle=\frac{t}{N}\sum{}'\exp\left(i\frac{e}{\hbar}\int_{\mathbf{C}}\vec{A}\cdot d\vec{r}_1\right)\times\exp(i\vec{k}\cdot\vec{R}_A-i\vec{k}'\cdot\vec{R}_B), \tag{A2}$$

where t is the hopping energy between two nearest-neighbor sites in the tight-binding scheme, the sum Σ' runs over the nearest-neighbor site pairs of A and B, and $\mathbf{C}$ denotes the path connecting the site pair.

Using the matrix element in Eq. (A2), one can estimate the effect of the magnetic field on the intervalley mixing. To do so, we assume that $\vec{k}$ and $\vec{k}'$ are located near the K and K' points, respectively. When a uniform magnetic field is applied, the path integration can be estimated, in terms of the magnetic length l_B and the lattice constant a, as $\frac{e}{\hbar}\int_{\mathbf{C}}\vec{A}(\vec{r}_1)\cdot d\vec{r}_1\sim a^2/l_B^2$. For

$$a^2/l_B^2\ll|\vec{K}-\vec{K}'|a, \tag{A3}$$

the intervalley mixing is negligible, since $\langle\Phi_{\vec{k}'}^{B}|H|\Phi_{\vec{k}}^{A}\rangle\simeq(t/N)\Sigma' e^{i\vec{k}\cdot\vec{R}_A-i\vec{k}'\cdot\vec{R}_B}\propto\delta(\vec{k}-\vec{k}')$. For the uniform field (perpendicular to the graphene sheet) of strength 10 T, one can find $a/(l_B^2|K-K'|)\sim10^{-4}$ so that the condition (A3) is achieved, which is why the intervalley scattering can be ignored in current experimental studies. The intervalley mixing becomes important in a very strong magnetic field $\sim10^4$ T, where $a/(l_B^2|K-K'|)\sim0.1$.

In the same way, one can find the condition when the intervalley mixing is negligible in a nonuniform field with constant gradient $\lambda=\nabla B(\vec{r})$. For the mixing to be ignored, the maximum value of the field must satisfy the condition (A3). In addition, the gradient λ should be much smaller than 10^4 T A^{-1}, since the path integration $(e/\hbar)\int_{\mathbf{C}}\vec{A}\cdot d\vec{r}_1$ in Eq. (A2) becomes comparable to $\vec{K}\cdot\vec{R}_A-\vec{K}'\cdot\vec{R}_B$ when $\lambda=\lambda_0\simeq1.7\times10^4$ T A^{-1}. In current experimental studies, the gradient is much smaller than λ_0 so that one can ignore the intervalley scattering.

APPENDIX B: TRANSMISSION THROUGH A GRAPHENE RIBBON INTERFEROMETRY

In this section, we derive the transmission probability through the inteferometry in Fig. 5(a), based on the scatter-

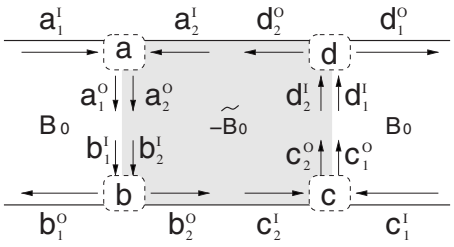

FIG. 6. The same as Fig. 5(a) but with detailed labeling of edge channels (represented by solid arrows) at its four scattering points $p \in \{a,b,c,d\}$ (dashed boxes). At each point p, there are two incoming channels with amplitude $(p_1^{\mathrm{I}},p_2^{\mathrm{I}})$ and two outgoing ones with $(p_1^{\mathrm{O}},p_2^{\mathrm{O}})$.

ing matrix formalism. The resulting expression in Eq. (B7) can describe the Aharonov–Bohm effect of the interferometry. One can easily obtain the transmission probability for other setups with different edge-channel configurations by slightly modifying the derivation.

The interferometry is in the integer quantum Hall regime so that its electron transport can be described by edge channels, such as the edge states along ribbon edges and the magnetic edge states along the boundaries $\overline{ab}$ and $\overline{cd}$. The scattering between the edge channels occurs at four scattering points $p \in \{a,b,c,d\}$. Each point p has two incoming channels with amplitude $(p_1^{\mathrm{I}},p_2^{\mathrm{I}})$ and two outgoing ones with $(p_1^{\mathrm{O}},p_2^{\mathrm{O}})$. For example, the two incoming channels to the point a are one right-going channel and the other left-going channel along the upper ribbon edge, while the two outgoing channels from a are the two magnetic edge channels along the line $\overline{ab}$ (see Fig. 6). At each point p, we introduce a scattering matrix S_p which links the amplitudes of the incoming and outgoing states,

$$\begin{pmatrix} p_1^{\mathrm{O}} \\ p_2^{\mathrm{O}} \end{pmatrix} = S_p \begin{pmatrix} p_1^{\mathrm{I}} \\ p_2^{\mathrm{I}} \end{pmatrix} = \begin{pmatrix} s_{11}^p & s_{12}^p \\ s_{21}^p & s_{22}^p \end{pmatrix} \begin{pmatrix} p_1^{\mathrm{I}} \\ p_2^{\mathrm{I}} \end{pmatrix}. \tag{B1}$$

The scattering matrix S_p has the general form of a 2×2 unitary matrix,

$$\begin{pmatrix} s_{11}^p & s_{12}^p \\ s_{21}^p & s_{22}^p \end{pmatrix} = e^{i\theta_p} \begin{pmatrix} i\sqrt{1-t_p^2}e^{i\phi_p} & t_p e^{i\phi_p'} \\ t_p e^{-i\phi_p'} & i\sqrt{1-t_p^2}e^{-i\phi_p} \end{pmatrix}. \tag{B2}$$

On the other hand, while edge channels propagate from one scattering point p to its neighboring point p', they acquire phase accumulation $\varphi_{pp'}$. As a result, one has

$$(b_1^{\mathrm{I}},b_2^{\mathrm{I}}) = e^{i\varphi_{ba}}(a_1^{\mathrm{O}},a_2^{\mathrm{O}}), \tag{B3}$$

$$(d_1^{\mathrm{I}},d_2^{\mathrm{I}}) = e^{i\varphi_{dc}}(c_1^{\mathrm{O}},c_2^{\mathrm{O}}), \tag{B4}$$

$$c_2^{\mathrm{I}} = e^{i\varphi_{cb}}b_2^{\mathrm{O}}, \tag{B5}$$

$$a_2^{\mathrm{I}} = e^{i\varphi_{ad}}d_2^{\mathrm{O}}. \tag{B6}$$

By combining the relations (B1)–(B6) and by setting $a_1^{\mathrm{I}}=1$ and $c_1^{\mathrm{I}}=0$, one can obtain the transmission probability $T=|d_1^{\mathrm{O}}|^2$ of the edge state incoming from the source (the left of the inteferometry) to the drain (the right),

$$T = \left| \frac{(t_b r_a + t_a r_b e^{-i\alpha})(t_c r_d + t_d r_c e^{-i\beta})}{1 - e^{i\varphi}(t_a t_b - r_a r_b e^{-i\alpha})(t_c t_d - r_c r_d e^{-i\beta})} \right|^2, \tag{B7}$$

where $r_p=\sqrt{1-t_p^2}$, φ contains the Aharonov–Bohm phase as well as the dynamical phase accumulated along one circulation of the closed loop $abcd$,

$$\varphi = \varphi_{ba} + \varphi_{cb} + \varphi_{dc} + \varphi_{ad} + \phi_a' - \phi_b' + \phi_c' - \phi_d' + \sum_{p\in\{a,b,c,d\}} \theta_p, \tag{B8}$$

$\alpha=\phi_a+\phi_b+\phi_a'-\phi_b'$, and $\beta=\phi_c+\phi_d+\phi_c'-\phi_d'$. The transmission T can describe the Aharonov–Bohm oscillation of the Dirac fermions in the setup of Fig. 5(a) as a function of $\tilde{B}$. Note that, in general, the scattering matrix S_p contains information on the scattering between the K and K' valleys.[36]

We close this appendix by analyzing Eq. (B7) for a simple case of $t_a=t_b=t_c=t_d=t=1/\sqrt{2}$. In this case, the transmission probability can be simplified as

$$T = \frac{\cos^2\frac{\alpha}{2}\cos^2\frac{\beta}{2}}{1 + 2\sin\frac{\alpha}{2}\sin\frac{\beta}{2}\cos\left(\varphi - \frac{\alpha}{2} - \frac{\beta}{2}\right) + \sin^2\frac{\alpha}{2}\sin^2\frac{\beta}{2}}. \tag{B9}$$

This result shows the usual form for the Aharonov–Bohm interference, except for the factors $\cos\alpha/2\cos\beta/2$ and $\sin\alpha/2\sin\beta/2$. From the factors, one can see that there appears no interference whenever $\alpha=\pi$ or $\beta=\pi$. It happens when destructive interference occurs during the propagation from one ribbon edge to the other through the two magnetic edge channels along $\overline{ab}$ or $\overline{cd}$ in such special cases.

[1] G. W. Semenoff, Phys. Rev. Lett. **53**, 2449 (1984).
[2] F. D. M. Haldane, Phys. Rev. Lett. **61**, 2015 (1988).
[3] K. S. Novoselov, A. K. Geim, S. V. Morozov, M. I. Katsnelson, I. V. Grigorieva, S. V. Dubonos, and A. A. Firsov, Nature (London) **438**, 197 (2005).
[4] Y. Zhang, Y. W. Tan, H. L. Stormer, and P. Kim, Nature (London) **438**, 201 (2005).
[5] See, e.g., T. Chakraborty and P. Pietiläinen, *The Quantum Hall Effects: Integral and Fractional* (Springer, New York, 1995).
[6] C. Berger, Z. Song, X. Li, X. Wu, N. Brown, C. Naud, D. Mayou, T. Li, J. Hass, A. N. Marchenkov, E. H. Conrad, P. N. First, and W. A. de Heer, Science **312**, 1191 (2006).
[7] F. Miao, S. Wijeratne, Y. Zhang, U. C. Coskun, W. Bao, and C. N. Lau, Science **317**, 1530 (2007).
[8] R. G. Mints, JETP Lett. **9**, 387 (1969).
[9] J. E. Müller, Phys. Rev. Lett. **68**, 385 (1992).

[10] H.-S. Sim, K.-H. Ahn, K. J. Chang, G. Ihm, N. Kim, and S. J. Lee, Phys. Rev. Lett. **80**, 1501 (1998).
[11] B. I. Halperin, Phys. Rev. B **25**, 2185 (1982).
[12] A. Nogaret, S. J. Bending, and M. Henini, Phys. Rev. Lett. **84**, 2231 (2000).
[13] F. M. Peeters and A. Matulis, Phys. Rev. B **48**, 15166 (1993).
[14] S. M. Badalyan and F. M. Peeters, Phys. Rev. B **64**, 155303 (2001).
[15] J. Reijniers, A. Matulis, K. Chang, F. M. Peeters, and P. Vasilopoulos, Europhys. Lett. **59**, 749 (2002).
[16] J. Reijniers, F. M. Peeters, and A. Matulis, Phys. Rev. B **59**, 2817 (1999).
[17] K. S. Novoselov, A. K. Geim, S. V. Dubonos, Y. G. Cornelissens, F. M. Peeters, and J. C. Maan, Phys. Rev. B **65**, 233312 (2002).
[18] N. Kim, G. Ihm, H.-S. Sim, and K. J. Chang, Phys. Rev. B **60**, 8767 (1999).
[19] H. A. Carmona, A. K. Geim, A. Nogaret, P. C. Main, T. J. Foster, M. Henini, S. P. Beaumont, and M. G. Blamire, Phys. Rev. Lett. **74**, 3009 (1995).
[20] P. D. Ye, D. Weiss, R. R. Gerhardts, M. Seeger, K. von Klitzing, K. Eberl, and H. Nickel, Phys. Rev. Lett. **74**, 3013 (1995).
[21] I. S. Ibrahim and F. M. Peeters, Phys. Rev. B **52**, 17321 (1995).
[22] A. Matulis, F. M. Peeters, and P. Vasilopoulos, Phys. Rev. Lett. **72**, 1518 (1994).
[23] H.-S. Sim, G. Ihm, N. Kim, and K. J. Chang, Phys. Rev. Lett. **87**, 146601 (2001).
[24] A nonuniform magnetic field has been generated by applying a uniform field to a nonplanar 2D system. See, e.g., M. L. Leadbeater, C. L. Foden, J. H. Burroughes, M. Pepper, T. M. Burke, L. L. Wang, M. P. Grimshaw, and D. A. Ritchie, Phys. Rev. B **52**, R8629 (1995).
[25] A. De Martino, L. Dell'Anna, and R. Egger, Phys. Rev. Lett. **98**, 066802 (2007).
[26] N. N. Lebedev, *Special Functions and Their Applications* (Dover, NewYork, 1972).
[27] In the presence of the step potential, V^j_{eff} depends on the eigenenergy E of the Dirac Hamiltonian in Eq. (2); for example, one finds $V^{j=A}_{\text{eff}}=[(x+k)^2/2]+(1/2)+2EV_0-V_0^2$ for $x<0$. As a result, V^j_{eff} should be studied in a self-consistent way [see Eq. (5)].
[28] L. Brey and H. A. Fertig, Phys. Rev. B **73**, 195408 (2006).
[29] See, e.g., R. Saito, G. Dresselhaus, and M. S. Dresselhaus, *Physical Properties of Carbon Nanotubes* (Imperial College Press, London, 1998).
[30] Y. Meir and N. S. Wingreen, Phys. Rev. Lett. **68**, 2512 (1992).
[31] S. Datta, *Electronic Transport in Mesoscopic Systems* (Cambridge University Press, Cambridge, England, 1995).
[32] H.-S. Sim, C.-J. Park, and K. J. Chang, Phys. Rev. B **63**, 073402 (2001).
[33] D. A. Abanin, P. A. Lee, and L. S. Levitov, Phys. Rev. Lett. **96**, 176803 (2006).
[34] L. Oriszlány, P. Rakyta, A. Kormányos, C. J. Lambert, and J. Cserti, Phys. Rev. B **77**, 081403(R) (2008).
[35] T. K. Ghosh, A. De Martino, W. Häusler, L. Dell'Anna, and R. Egger, Phys. Rev. B **77**, 081404(R) (2008).
[36] The scattering between the valleys K and K' has been studied in a graphene ribbon. See, e.g., J. Tworzydlo, I. Snyman, A. R. Akhmerov, and C. W. J. Beenakker, Phys. Rev. B **76**, 035411 (2007).